Proceedings of the
Annual Stability Conference
Structural Stability Research Council
Louisville, Kentucky, April 1-4, 2025

O.I.C.-based design of steel H.S.S. at high temperatures

Gabrielle Pomerleau[1], Mina Aleseyedan[2], Pablo Rico[3], Mariana Echeverri [4], Nicolas Boissonnade[5]

Abstract

This paper investigates the cross-sectional fire resistance of hot-rolled rectangular or square hollow section shapes. Advanced non-linear shell F.E. models are first developed then validated against 17 carefully-conducted and documented tests. These tests included Class 2 (plastic) and Class 4 (slender) tube sections of square and rectangular section under combined compression and bending configurations, under temperatures spanning from 20°C to 700°C. As an excellent agreement between the numerical predictions and the reference test data is evidenced, the F.E. models have been extensively used to characterize the cross-sectional behaviour and resistance of such tubes under fire. The results of some 1 400+ non-linear simulations have been collected to characterize the influences of (i) the cross-section geometry and shape (including the response to local buckling), (ii) temperature and (iii) load arrangement (simple or combined).

Besides, a novel design approach based on the Overall Interaction Concept (O.I.C.) has been developed. Beyond offering more simple and straightforward design verifications, the proposal is seen to provide much more accurate and consistent resistance predictions than current design specifications such as Eurocode 3, the American or the Canadian specifications. Indeed, while Eurocode 3 predictions are usually safe-sided, both American A.I.S.C. and Canadian CSA-S16 recommendations often lead to optimistic, unsafe results, whereas the O.I.C.-based proposal remains safe-sided and precise. Eventually, reliability analyses further evidence the proposed approach to offer a very good safety level, quite above current design rules.

1. Introduction

The present paper deals with the behaviour and resistance of steel tubular sections exposed to fire. More precisely, focus is here on the resistance to compression and/or bending of hot-rolled square or rectangular hot-rolled tubes at high temperatures. Within a fire, steel material properties are known to decline rapidly and to affect resistance in multiple ways: indeed, when heated above 500°C – which is not uncommon in fire situations –, both the yield stress f_y and the Young's

[1] MSc student, Laval University, <gabrielle.pomerleau.4@ulaval.ca>
[2] MSc student, Laval University, <minaaleseyedan@gmail.com>
[3] PhD student, Laval University, <pablo.rico.1@ulaval.ca>
[4] PhD student, Laval University, <mariana.echeverri-loaiza.1@ulaval.ca>
[5] Professor, Laval University, <nicolas.boissonnade@gci.ulaval.ca>

modulus E are significantly reduced ((Kodur, 2010), (Knobloch, 2014), (Franssen, 2015) (European Committee for Standardisation, 2020) (AISC, 2016)). Moreover, the σ-ε material relationship becomes significantly non-linear, in addition to seeing the plastic plateau vanish. As a result, the resistance and stability response of hollow section shapes under fire is notably affected, and usual design formulae dedicated to steel sections or members at room temperature cannot be straightforwardly adapted to fire design by merely adjusting material properties.

Our objective here consists of presenting an original, innovative design approach for such square and rectangular tubular sections at high temperatures. The fire design of steel structures did not receive sustained attention prior to the 1950's, and structures were primarily designed for "normal loads" so that fire design was considered a secondary issue. Yet, the behaviour and design of steel sections and elements has received much deeper attention in recent decades; as particular points, most authors report (i) important reductions in resistance owing to the high temperatures as well as (ii) the need to develop specific design methodologies. As examples, one may refer to the investigations of Pauli et al. ((Pauli, 2012) (Pauli, 2013)), were significant reductions in resistance compared to the room temperature situation are reported. Too, a quite significant importance of local buckling – detrimental – effects is reported, as a consequence of the Young's modulus E to decrease faster than the yield stress f_y with temperature, hence the greater sensitivity to local buckling ((Knobloch, 2007) (Knobloch, 2013) (Quiel, 2010) (Somaini, 2012) (Couto, 2015) (Fang, 2019) (Kucukler, 2021)). To address these challenges, many researchers have adopted the concept of the Effective Width Method (E.W.M., (Von Karman, 1932) (Winter, 1947)) and adapted it to fire situations ((Couto, 2014) (Knobloch, 2006) (Renaud, 2006) (Quiel, 2010)). As a consequence, major design codes for the fire design of steel structures ((European Committee for Standardisation, 2020) (AISC, 2016)) rely on the E.W.M. Yet, recent research ((Couto, 2015) (Fag, 2019) (Couto, 2016) (Yun, 2020) (Couto, 2021)) evidence issues – inaccurate and inconsistent resistance predictions – in these standard when it comes to account for the non-linear stress-strain relationship of steel at high temperatures. Besides, alternative methods such as the Continuous Strength Method (C.S.M., (Yun, 2020) (Afshan, 2013) (Theofanous, 2016)) or the Direct Strength Method (D.S.M., (Couto, 2021) (Fang, 2018) (Chen, 2008)) have been extended to fire scenarios but still need improvements.

This paper aims at presenting an original design approach capable of addressing all the issues and shortcomings briefly described previously. Based on the principles of the O.I.C. (Boissonnade, 2017), the proposed approach aims at providing:

(i) More accurate and consistent design resistance predictions;
(ii) A more simple, practical and direct approach, without resorting to the Effective Width Method nor to the classification concept;
(iii) A sound theoretical framework based on the well-known resistance-instability interaction, treated through convenient slenderness-reduction factor relationships;
(iv) A proper handling of the non-linear response of steel at high temperatures.

In this respect, the methodology relied upon in this paper first details the development of advanced and suitable shell F.E. models (§ 2.1). Such models are evidenced to accurately and adequately provide reliable resistance estimates through a validation study described in Section 2.2. As excellent agreement with experimental sources is evidenced, the numerical models have been used extensively to gather a large number of reference results; the latter have been employed to assess the merits of an O.I.C.-based proposal (Section 3), which is detailed along Section 4. This last section further assesses the performance of the proposed design equations against the reference

numerical F.E. results; also, the proposed design approach is compared to both existing design recommendations and to the F.E. results. Eventually, safety studies towards the determination of a suitable partial safety factor to be associated to the proposed design equations are detailed.

2 Development and assessment of Finite Element models

2.1 General modelling assumptions

Shell finite element models have been developed within software ABAQUS (Abaqus, 2011). Typical quadrangular shell elements with four nodes and reduced integration (S4R element) have been used. This shell element features a classical Bernouilli/Kirchhoff assumption and was used with 7 integration points across the thickness. All non-linear analyses have been conducted through state-of-the-art numerical techniques, i.e., a combined Newton-Raphson/Riks approach in Updated Lagrangian Formulation. This was coupled with automatic time stepping strategies up to collapse and beyond within G.M.N.I.A. calculations (Geometrically and Materially Non-linear with imperfection Analyses). As for critical load calculations (L.B.A., Linear Buckling Analyses), typical Lanczos or subspace iteration numerical methods have been employed.

Preliminary mesh density studies were also conducted, where the aspect ratios of the shell elements never exceeded 2.0 (Fig. 1). Such studies allowed to identify the best compromise between accuracy of the F.E. solution and computation time. Typical coarse (Type 1), intermediate (Types 2 to 5) or refined (Type 6) meshes have been considered along L.B.A. and G.M.N.I.A. calculations, for different cross-section shapes and geometries, material grades and temperatures. One example of results is provided in Fig. 2, where it is observed that mesh Types 4-5 provide quite accurate results compared to mesh Type 6 (exaggeratedly dense), kept as a reference. Accordingly, mesh Type 4 was finally chosen along the numerical studies as the one offering the best precision for a reasonable computation effort.

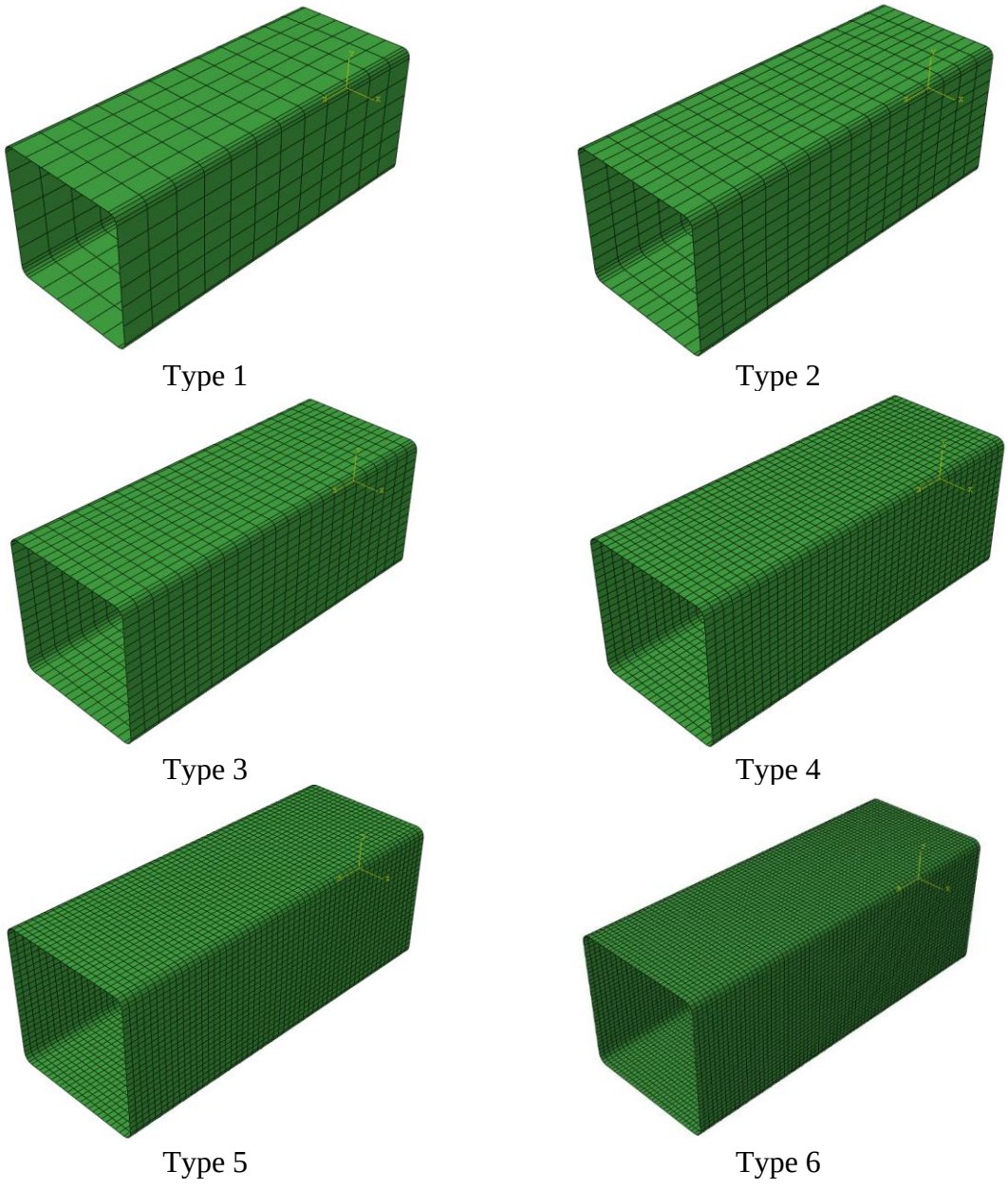

Figure 1: Meshes considered for square hollow sections.

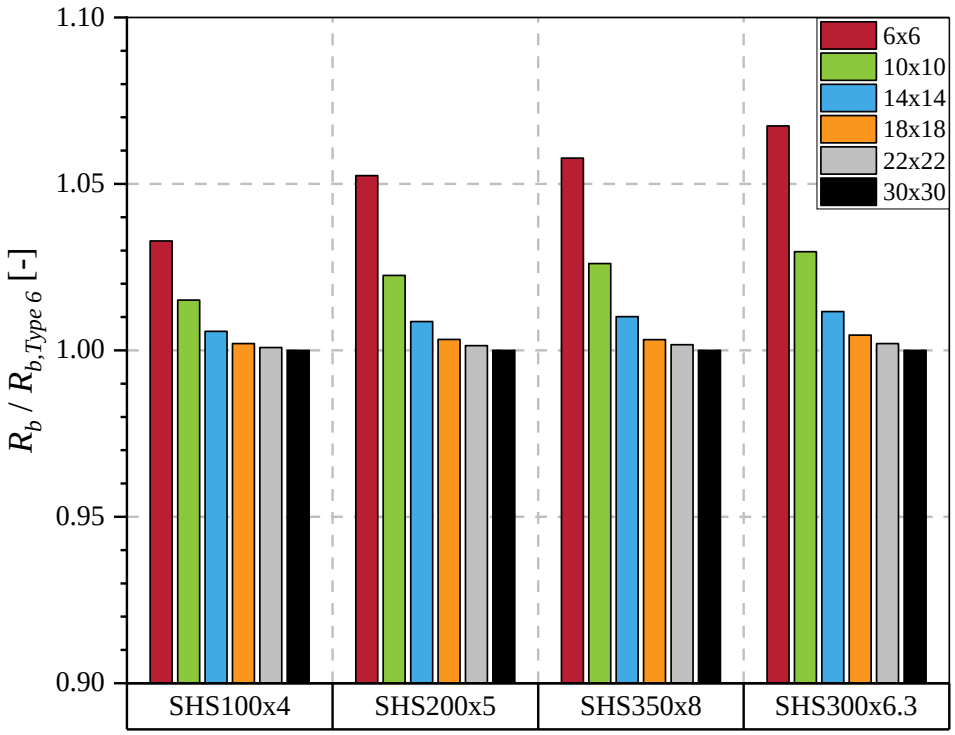

Figure 2: Mesh sensitivity results for square sections in compression (f_y = 350 *MPa* and θ = 700°C).

Material laws for temperatures above 400°C have been adopted in compliance with the recommendations of Eurocode 3, cf. Fig. 3a. They account for (i) an early elastic linear response followed by (ii) a curved response (elliptic equation) up to the yield stress $f_{y,\theta}$, then by (iii) a plastic plateau and finally (iv) a linear decreasing part down to the ultimate strain $\varepsilon_{u,\theta}$. Obviously, all parameters of this material response are temperature-dependant (e.g., yield stress $f_{y,\theta}$ and E_θ depend on the temperature θ) and allow to account for all important effects of temperature on the material response ((Kodur, 2010) (Franssen, 2015) (Knobloch, 2013)): loss in stiffness and in yield stress as well as a more pronounced non-linear pattern at the onset of yielding – loss in proportionality. In the Eurocode 3 framework (European Committee for Standardisation, 2020), these effects are accounted for through reduction factors $k_{y,\theta}$, $k_{E,\theta}$ and $k_{p,\theta}$, respectively; these factors are defined as a function of the temperature and shall multiply – reduce – the reference 20°C steel properties to get the fire ones, e.g., $f_{y,\theta} = k_{y,\theta} \cdot f_{y,20°C}$. For lower temperatures (θ < 400°C), typical Fig. 3b patterns were adopted; this alternative model is proposed in Annex A of EN 1993-1-2 (European Committee for Standardisation, 2020) and also suggested by Yun et al. (Yun, 2020), in an effort to take into account strain-hardening further to 2% strain. The detailed equations of the strain-hardening part can be found in (European Committee for Standardisation, 2020).

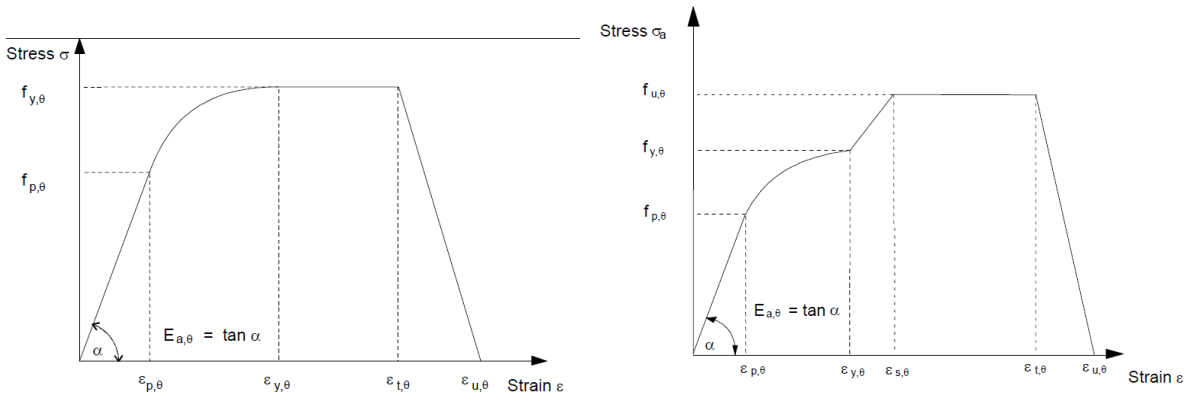

Figure 3: Stress-strain curves for carbon steel at high temperatures – a) For $\theta > 400°C$ – b) For $\theta < 400°C$.

As only hot-rolled tubes are considered in this study, radii were defined as mid-thickness radii $r = 1.5 \cdot t$ where t represents the thickness. When F.E. results have been compared to test data (cf. § 2.2), geometries matching exactly those measured in tests have considered; also, boundary conditions have been defined as closely as possible to real experimental ones.

Besides, along parametric studies (§ 2.3), boundary conditions have been implemented so as to replicate beam theory-like simply supported ones. First, displacements perpendicular to the flat part of end sections were prevented, in order to prevent local buckling and/or load bearing failures in these areas. Then, a series of kinematic constraints has been applied to both end sections which forces the end nodes to respect the typical "plane sections remain plane" Bernoulli assumption, so that each end section may posses a maximum of 3 cross-sectional deformation modes: axial displacement and major + minor axis rotations. This modelling technique could be shown ((Nseir, 2015a) (Hayeck, 2016) (Aleseyedan, 2023) (Li, 2023a) (Gerard, 2021) (Hayeck, 2017) (Nseir, 2015b)) to avoid stress concentrations and to offer excellent convergence properties. Finally, fictitious nodes were created at the centres of the tube's end sections to apply vertical and horizontal supports.

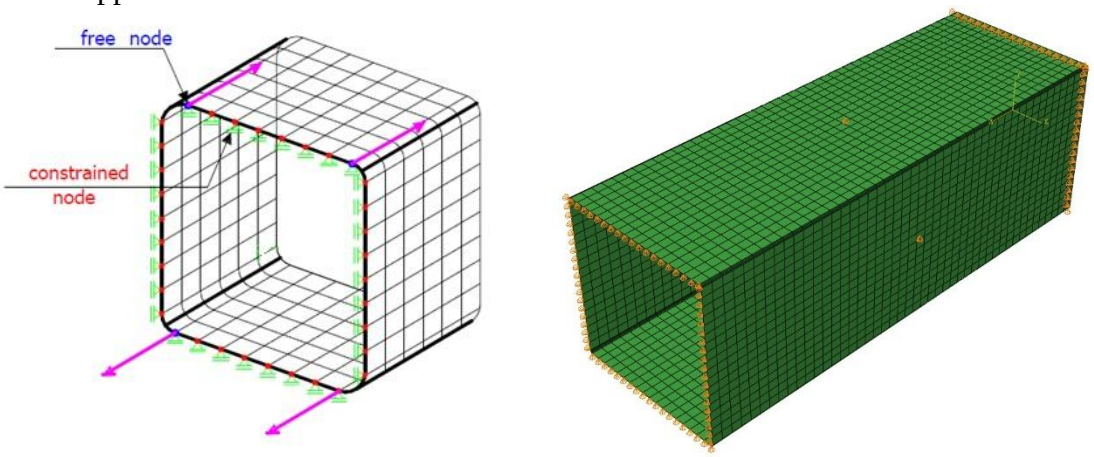

Figure 4: a) Illustration of kinematic constraints and load application – b) Additional transverse fixities at end-sections.

Loading was applied consistently with the adopted support conditions and defined as 4-point loads acting at edge nodes in the upper and lower plates, see Fig. 4a. Thanks to the kinematic conditions, this allowed to prevent stress concentrations and distribute loading evenly along the sections.

Through adequate distributions of each of these 4 forces, all types of loading situations were possible: simple compression or bending, as well as combined loading situations.

For compression and bending load combinations, loading was always applied proportionally. Further load path sensitivity studies ((Nseir, 2015a), (Hayeck, 2016)) have indeed shown that this sequence leads to the most reliable results.

As for imperfections, no residual stresses where actually accounted for: previous research ((Franssen, 2015) (Pauli, 2013) (Couto, 2015) (Couto, 2016) (Yun, 2020) (Yang, 2009 (Ng, 2007) (Vila Real, 2004)) indeed has established that many factors (e.g., strain and heating rate, temperature levels, duration of exposure to fire, …) affect the distribution of residual stresses in fire situations. They can be shown to be considerably released at high temperatures, as confirmed by the failure behavior of stub columns ((Yang, 2009) (Ng, 2007)). Accordingly, and following the recommendations of Yun et al. (Yun, 2020) and Pauli (Pauli, 2013) on their numerical models, the effect of residual stresses on the resistance of sections in fire was ignored.

Eventually, local geometrical imperfections were accounted for in the models, by means of adequate modifications of node coordinates, i.e., without relying on eigenshapes. A total of 3 sine-based half-wave patterns were defined in both directions of each plate, characterised by (i) a half-wavelength defined as the average flat width of the flange $a_f = b - t - 2 \cdot r$ and of the web $a_w = h - t - 2 \cdot r$ and by (ii) an amplitude equal to $a_w / 200$ for the webs and $a_f / 200$ for the flanges – see Fig. 5b for a magnified view of the adopted local imperfections. These values have been previously investigated by Nseir et al. (Nseir, 2016) and proved adequate. As for validations studies (next paragraph), measured amplitudes were considered in the numerical models.

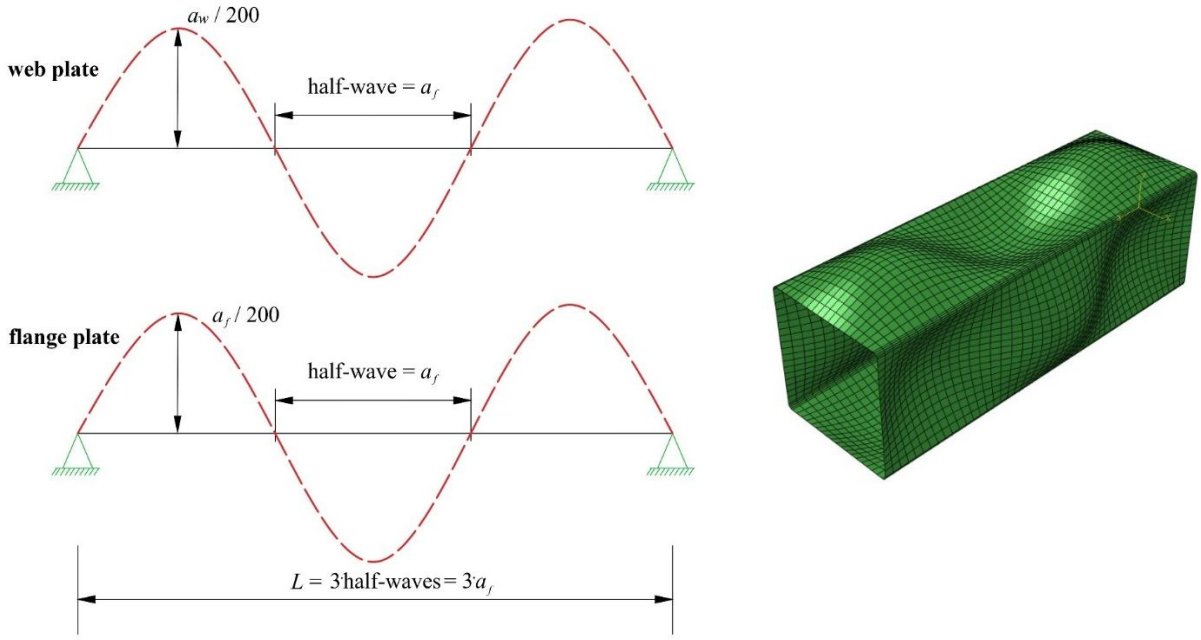

Figure 5: Local imperfections – a) Definition of wavelength and amplitude – b) Overall view of initial imperfect geometry of F.E. mesh (magnified).

2.2 Validation of numerical models against experimental data

The ability of the shell F.E. models to provide reliable resistance predictions has been tested against the well-documented test series of Pauli ((Pauli, 2012), (Pauli, 2013)), and the details of the validation are provided in this section. The primary objective remains to evidence that the numerical models can be deemed equivalent to physical testing, so they can be extensively used within numerical parametric studies (§ 2.3).

The detailed reports of Pauli et al. relate to a series of 17 fire tests on 10 RHS and 7 SHS and provide all necessary information for an accurate numerical modelling, namely (i) full stress-strain measured relationships, (ii) actual geometries and dimensions (in particular thickness t), (iii) detailed support conditions, (iv) accurately measured geometrical imperfections and (v) observations during testing. All such data have been carefully introduced in the shell F.E. models and Table 1 provides a summary comparison between measured peak loads and F.E. predictions. Fig. 6 also reports graphically on the prediction performance of the shell models with respect to experimental results.

Table 1: Comparison of F.E.-predicted to measured failure loads.

Name of specimen	Temperature [$°C$]	Experimental ultimate load [kN]	Numerical ultimate load [kN]	$N_{F.E.}$ / N_{test} [–]
S1	550	364	366	1.00
S2	550	403	367	0.91
S3	400	795	760	0.96
S4	20	1225	1176	0.96
S5	700	138	126	0.91
S6	550	468	451	0.96
S7	700	88	93	1.05
S01	400	280	234	0.84
S02	400	408	336	0.82
S03	550	257	209	0.81
S04	550	205	152	0.74
S05	20	356	322	0.91
S06	700	74	69	0.93
S07	20	483	445	0.92
S08	550	87	72	0.83
S09	400	133	114	0.85
S10	20	161	150	0.93
			Average	**0.90**
			C.o.V.	**0.09**
			Average excluding S04 + S08	***0.92***
			C.o.V.	***0.07***

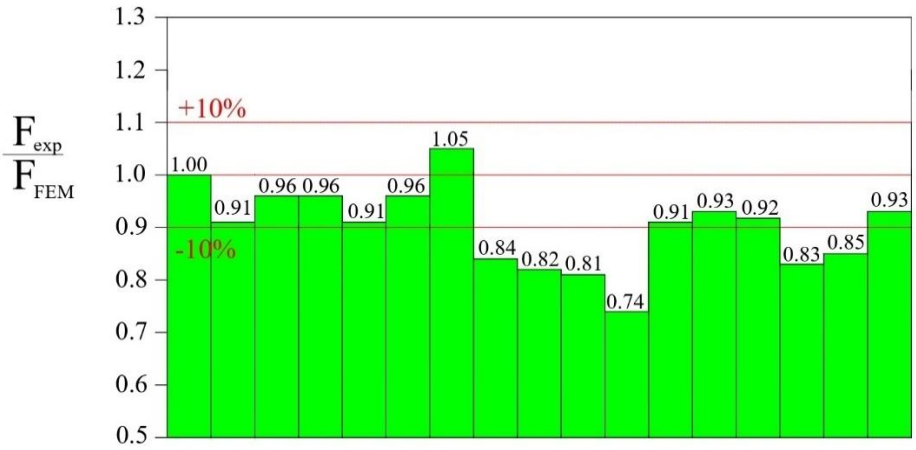

Figure 6: Experimental vs numerical peak loads.

As can be seen, quite good agreement between both sources is reported. Moreover, in their reports, Pauli et al. explain that tests S04 and S08 exhibited an unusual level of rotational restraint at the end supports (frictional issues, cf. (Pauli, 2012)) so that these tests results may have unexpectedly reached too high peak loads. Therefore, Table 1 also reports mean and Coefficient of Variation values of the ratio $N_{F.E.}$ / N_{test} when these two tests are excluded from the comparison. As a mean value of 0.92 associated to a C.o.V. of 7% is reported, it is concluded that the F.E. models possess an excellent ability to predict failure loads at high temperatures, given the variations considered in temperature, cross-sectional shape, load arrangement, etc. Also, fire testing is more delicate and sensitive than room temperature testing, so that these values are very acceptable. Further, Fig. 7a provides an example of load-displacement response where the experimental record is compared to the numerically-predicted one. It is observed that the F.E. model is also capable of satisfactorily predicting (i) the general shape of the curve, (ii) the elastic response and (iii) the post-peak behaviour. As Fig. 7b further shows, failure modes have also been satisfactorily captured. In conclusion, the numerical models are proved fully adequate, accurate and reliable enough to be safely substituted to physical testing.

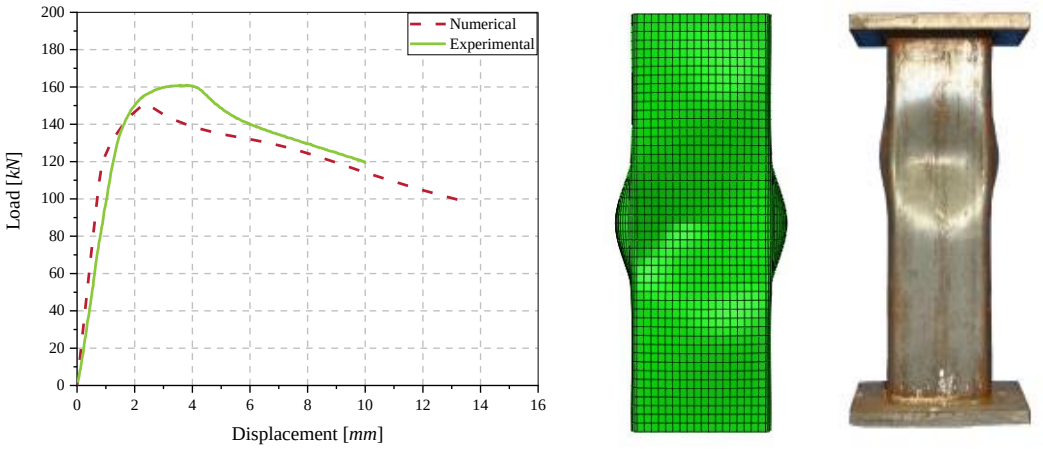

Figure 7: Results for specimen S10 – a) Full load-displacement curves – b) Comparison of numerical vs experimental failure shape.

2.3 F.E. parametric studies

The numerical tools being proved adequate, they have been used extensively to gather a large dataset of reference results. A total of 1 404 F.E. results has been brought together, varying different parameters as follows:

- Cross-section shape and geometry: 36 different sections have been considered (12 square SHS + 24 rectangular RHS), with dimensions from 50 x 150 *mm* to 450 x 450 *mm*;
- Thickness *t*: thickness was varied from 3.85 *mm* to 22.5 *mm* so as to vary plate section slenderness *h* / *t* (or *b* / *t*) from 6 to 90, i.e., very compact to very slender section geometries have been studied (see also details in Table 2);
- Temperatures were chosen as 350℃, 550℃, and 700℃ (uniform and constant temperature was considered in all sections). Choice has also been made to keep a series of simulations at 20°C (room temperature) to serve as a reference;
- Load case: either simple (compression *N*, major-axis-bending M_y or minor-axis bending M_z) or combined loading situations have been contemplated. A total of 10 combined load cases has been defined (see Table 3). They have been thought to span the entire set of possibilities for combined loading situations, and some cases are dominated by compression while others are bending-driven.

Table 2: geometrical dimensions of sections.

Shape	Width *b* [*mm*]	Height *h* [*mm*]	Thickness *t* [*mm*]	*b* / *t* [–]	*h* / *t* [–]
Rectangular	50	150	7.50	6.67	20.00
Rectangular	75	150	7.50	10.00	20.00
Square	150	150	7.50	20.00	20.00
Rectangular	100	300	15.00	6.67	20.00
Rectangular	150	300	15.00	10.00	20.00
Square	300	300	15.00	20.00	20.00
Rectangular	150	450	22.50	6.67	20.00
Rectangular	225	450	22.50	10.00	20.00
Square	450	450	22.50	20.00	20.00
Rectangular	50	150	3.85	12.99	38.96
Rectangular	75	150	3.85	19.48	38.96
Square	150	150	3.85	38.96	38.96
Rectangular	100	300	6.65	15.04	45.11
Rectangular	150	300	6.65	22.56	45.11
Square	300	300	6.65	45.11	45.11
Rectangular	150	450	10.00	15.00	45.00
Rectangular	225	450	10.00	22.50	45.00
Square	450	450	10.00	45.00	45.00
Rectangular	50	150	2.20	22.73	68.18
Rectangular	75	150	2.20	34.09	68.18
Square	150	150	2.20	68.18	68.18
Rectangular	100	300	4.40	22.73	68.18

Rectangular	150	300	4.40	34.09	68.18
Square	300	300	4.40	68.18	68.18
Rectangular	150	450	6.50	23.08	69.23
Rectangular	225	450	6.50	34.62	69.23
Square	450	450	6.50	69.23	69.23
Rectangular	50	150	1.60	31.25	93.75
Rectangular	75	150	1.60	46.88	93.75
Square	150	150	1.60	93.75	93.75
Rectangular	100	300	3.30	30.30	90.91
Rectangular	150	300	3.30	45.45	90.91
Square	300	300	3.30	90.91	90.91
Rectangular	150	450	4.95	30.30	90.91
Rectangular	225	450	4.95	45.45	90.91
Square	450	450	4.95	90.91	90.91

Table 3: combined load cases.

Load case	θ [°]	φ [°]	Dominant force
$N + M_y$	30	0	N
	60	0	M_y
$N + M_z$	30	90	N
	60	90	M_z
$M_y + M_z$	90	30	M_y
	90	60	M_z
$N + M_y + M_z$	30	30	N *and* M_y
	30	60	N *and* M_z
	60	30	M_y
	60	60	M_z

In addition to G.M.N.I.A. calculations, both M.N.A. (Materially Non-linear Analysis – Leading to R_{pl}, cf. § 3.1) and L.B.A. (Linear Buckling Analysis – Leading to $R_{cr,L}$) computations have performed, for a total of 5 616 non-linear shell F.E. analyses. The various features of the previously-described numerical models have been considered, yet a few aspects shall be mentioned here:

- Firstly, nominal values have been adopted all along the parametric studies, for material properties and geometrical dimensions;
- Supports have been defined as pinned-pinned ideal, beam-like conditions, as described and explained in § 2.1;
- Sets of "standard" imperfections have been adopted as follows: no residual stresses have been considered – cf. reasons detailed in § 2.1 – and local geometrical imperfections have been considered as 3 half-waves (Fig. 5a) with amplitudes as detailed in § 2.1.

All together, these 1 400+ reference G.M.N.I.A. F.E. simulations allow to study in detail the individual influence of a given parameter on the cross-sectional resistance of hollow sections in fire. Figs. 8a and 8b further allow to get an early view of some of the obtained F.E. results, as a function of temperature. In these figures, the horizontal axis λ_L refers to the relative *local* (L) slenderness and χ_L denotes the relative resistance; both include the decrease in mechanical properties owing to fire – further details and background information on χ_L and λ_L are provided in the next section. As can be seen, high temperature results are relatively scattered (and quite lower than room temperature 20°C ones), whatever the loading scenario. Also, no visible effect of the fire temperature considered seems to affect the observed scatter, i.e., data points are not "ordered" as a function of temperature. Consequently, changes in temperature cannot be deemed responsible for the observed dispersion, and another parameter responsible for the scatter still has to be identified.

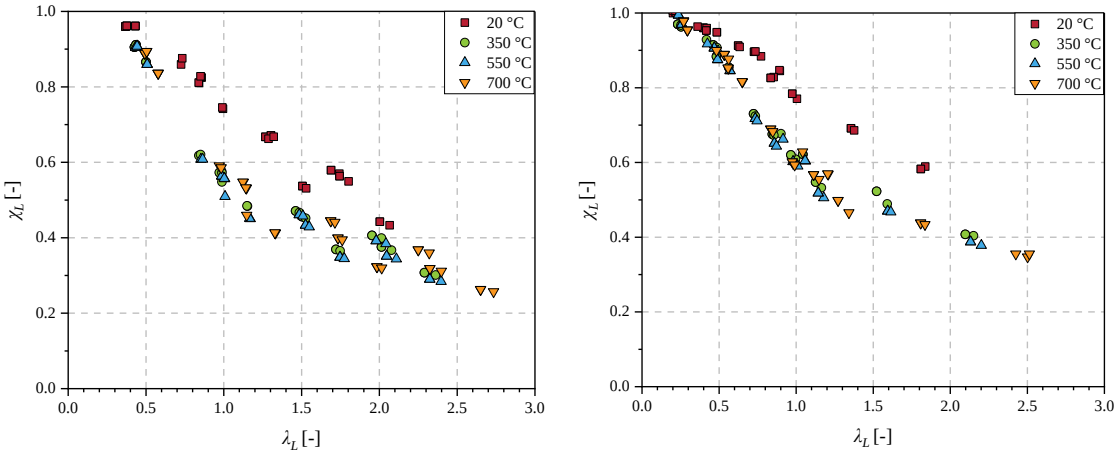

Figure 8: Evolution of $\chi_L = f°(\lambda_L)$ as a function of temperature – a) Section under compression N – b) Sections under major-axis bending M_y.

3. O.I.C. design proposals

3.1 Basic principles of the O.I.C.

The Overall Interaction concept (O.I.C.) is a slenderness-based design approach providing direct resistance estimates, either for cross-sections or for members ((Boissonnade, 2017), (Boissonnade, 2015), (Nseir, 2015c), (Boissonnade, 2014), (Nseir, 2014), (Boissonnade, 2013)). It allows for a simple yet accurate handling of the resistance – stability interaction (yielding vs local and/or member buckling) and further includes the influence of imperfections. More details may be found in (Boissonnade, 2017) for a deeper description of background principles and application steps to steel sections ((Li, 2022a), (Li, 2022b), (Li, 2022c), (Li, 2022d), (Gerard, 2021)), elements ((Li, 2022e), (Hayeck, 2018)), stainless steel (Gagne, 2020), aluminium structures ((Li, 2023b), (Li, 2023c)), fire design ((Li, 2023d), (Li, 2023e)), etc. In this paper, the O.I.C. approach is applied to predicting the carrying capacity of tubular cross-sections in fire. Obviously, the key principles and design steps remain identical, yet the way material properties decrease with temperature shall be properly accounted for. The basic concept of the O.I.C. relies on establishing a relationship between the relative slenderness λ and a reduction factor χ, that decreases the plastic capacity kept as a reference. This type of approach has successfully been adopted in major design codes for decades in the case of column buckling for example. In this paper, this approach is extended to (i)

cross-section, local (L) resistance under fire and to (ii) combined loading situations. The $\chi_L = f°(\lambda_L)$ relationship (local buckling curve, see Fig. 9) accounts for interactions between material yielding, local buckling and imperfections, as influenced by temperature.

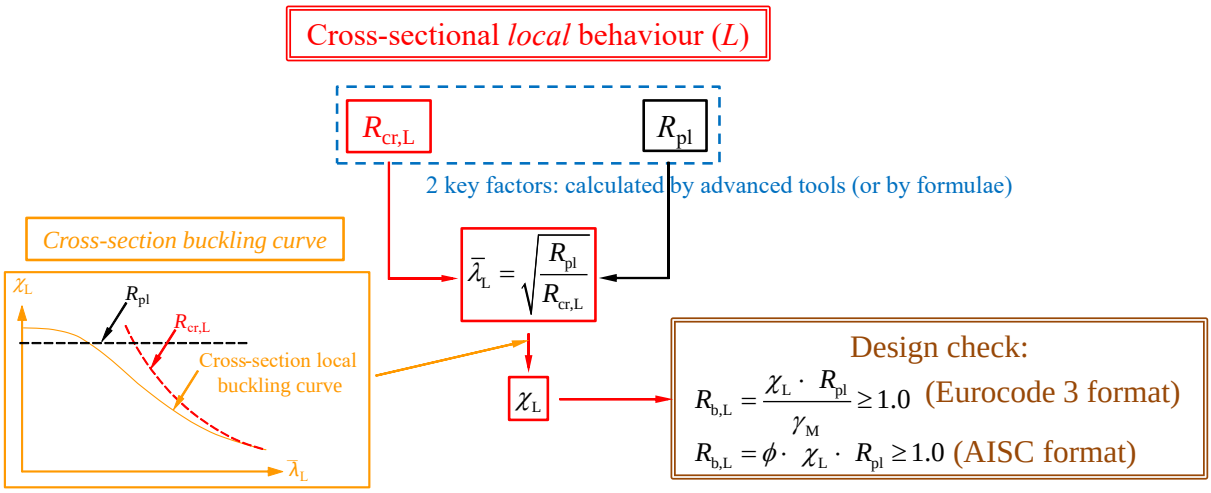

Figure 9: O.I.C. steps for cross-sectional behaviour.

Application of the O.I.C. to combined load cases relies on the use of so-called "*R* ratios" that stand as the *local critical* load ratio $R_{cr,L}$ and the *plastic* load ratio R_{pl}. $R_{cr,L}$ corresponds to the factor by which the (combined) initial set of loads shall be multiplied to reach the local buckling load level, whereas R_{pl} is the ratio by which the initial loading must be multiplied to attain the plastic capacity. Both R_{pl} and $R_{cr,L}$ load ratios where evaluated numerically with ABAQUS (see § 2.3) in the application of the O.I.C. approach considered here (Section 4).

$$\chi_L = \frac{1}{\phi_L + \sqrt{\phi_L^{\,2} - \bar{\lambda}_L^{\,\delta}}} \leq 1 \quad \text{where} \quad \phi_L = 0.5 \cdot \left[1 + \alpha_L \cdot \left(\bar{\lambda}_L - \lambda_0\right) + \bar{\lambda}_L^{\,\delta}\right] \qquad (1)$$

In the present study, a typical Ayrton-Perry format ((Ayrton, 1886), (Maquoi, 1978)) has been chosen (see Eq. (1)), to provide a general expression for the local buckling curve. In this respect, key coefficients are (i) λ_0, which stands as the slenderness "plateau length", i.e., the value of the local slenderness λ_L below which a full plastic resistance can be reached ($\chi_L \geq 1.0$), (ii) factor δ that aims at providing additional resistance owing to plate post-buckling effects for slender sections and (iii) α_L which is denoted as the equivalent local geometrical imperfection factor, i.e., α_L aims at accounting for the effect of the various imperfections to be considered. Combined with the definition of local relative slenderness λ_L as taking the balance between the plastic capacity R_{pl} and the $R_{cr,L}$ elastic stability limit cases, this format provides a strong mechanical basis to the O.I.C. approach, and the remaining coefficients in all previously-listed parameters shall be adjusted to the reference F.E. results, as a compromise between accuracy and simplicity. Furthermore, as Fig. 8a and 8b showed, the collected numerical results exhibit a certain scatter, as various factors can be evidenced to have an impact on resistance. Accordingly, a single, safe-sided, $\chi_L = f°(\lambda_L)$ buckling curve is deemed inappropriate, and a series of curves shall be preferred; this aspect is further detailed in § 3.2.

As a particular point, the proposed design approach for combined loading situations relies on the use of a 3D resistance surface, as shown in Fig. 10, which is defined in the n-m_y-m_z loading space

where the relative axial force $n = N_S / N_{pl}$ is the ratio of the applied compression N_S to the plastic axial resistance N_{pl}, m_y is the ratio between the applied major-axis bending moment $M_{y,S}$ to the plastic capacity $M_{pl,y}$ and $m_z = M_{z,S} / M_{pl,z}$. The basic idea here consists in (i) defining "anchor points" for pure n, m_y and m_z cases (they correspond to simple load cases and are characterized by individual reduction factors $\chi_{L,N}$, $\chi_{L,My}$ and $\chi_{L,Mz}$ – see red circles on Fig. 10a) and in (ii) adjusting globally and locally the shape of the 3D resistance surface that is based on these anchor points. Use of spherical coordinates is relevant here, and Eq. (2) provides the general expression leading to the combined reduction factor $\chi_{L,combined}$ as a function of anchor points $\chi_{L,N}$, $\chi_{L,My}$ and $\chi_{L,Mz}$ and angles θ and φ. In Eq. (2), factor q_1 aims at fine-tuning the general shape of the curve, while coefficients q_2 to q_6 intend at locally modifying the concave or convex nature of the surface; indeed, a concave shape is typically met in compression-dominated areas, as a consequence of strong geometrical 2nd order effects (local instability). In contrast, convex areas are usually observed in cases where yield extent leads over local buckling. All q-factors have been calibrated to best fit the reference numerical results – see also § 4.2; Fig. 10b provides an example of the influence of q_1 on the general shape of the surface, at different relative axial force n intervals.

$$\chi_{\mathrm{L,combined}} = \left[\left(\chi_{\mathrm{L},N} \cdot \cos^{q_2}\theta \right)^{q_1} + \left(\chi_{\mathrm{L},M_y} \cdot \sin^{q_3}\theta \cdot \cos^{q_4}\varphi \right)^{q_1} + \left(\chi_{\mathrm{L},M_z} \cdot \sin^{q_5}\theta \cdot \sin^{q_6}\varphi \right)^{q_1} \right]^{\frac{1}{q_1}} \quad (2)$$

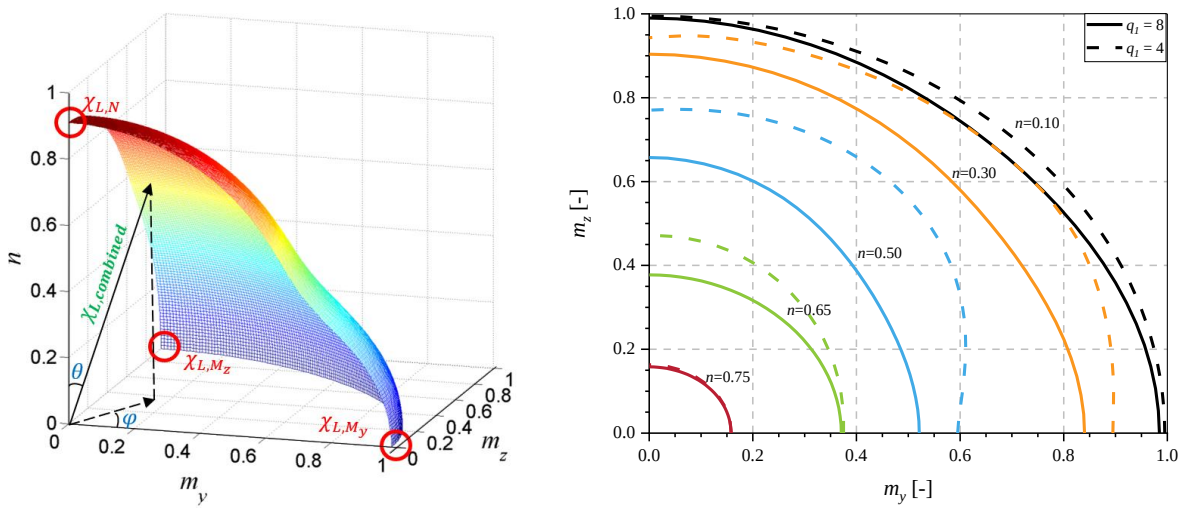

Figure 10: a) 3D resistance surface – b) Influence of factor q_1.

3.2 Identification of additional design parameters

As detailed previously, the main key factors having an influence on cross-section resistance (e.g., material properties, section geometry) are inherently taken into account within the O.I.C. approach, either through the critical load ratio $R_{cr,L}$ or the plastic load ratio R_{pl}. In particular, the decrease in material properties following heat exposure is accounted for. Yet, the influence of fire is only taken into account through modifications in Young's modulus E and yield stress f_y, so that the decrease in proportionality at the end of the elastic response (factor k_p) is not accounted for; also, both R_{pl} and $R_{cr,L}$ are relative to "limit cases", i.e., either only material yielding is accounted for (no local buckling nor imperfections) or only elastic buckling is described (no yielding and no imperfections), respectively. Accordingly, in real situations where all these effects can occur simultaneously, it may be necessary to account further for these and for the effect of imperfections, as many interactions between all these develop. As Fig. 8a and 8b show, the scatter in results

implies that a one-to-one $\chi_L = f°(\lambda_L)$ relationship is not appropriate, hence the need to identify one or more parameters responsible for this dispersion. Choice was made here to rely on a single factor to address this, striving for simplicity. This factor, denoted as γ (Eq. (3)), was identified as being of geometrical nature, with negligible dependence on material or on temperature. Therefore, it was proposed that dependency of the local buckling curves on γ be accounted for through factors $\alpha_L = f°(\gamma)$ and $\delta = f°(\gamma)$, as detailed in the next section.

$$\gamma = \frac{h \cdot b}{t^2} \tag{3}$$

3.3 O.I.C. design proposals

The 1 400+ F.E. reference results collected and detailed in § 2.3 have served as reference results for the calibration of design equations, following the O.I.C. framework. Eurocode 3 recommendations (European Committee for Standardisation, 2020) for the evolution of steel properties with temperature have been adopted, and Table 4 summarizes the values of λ_0, α_L and δ to be considered for simple load cases, while Table 5 provides the values of q-factors needed for combined load cases. Associated with Eqs. (1) to (3) and the O.I.C. steps (Fig. 9), these expressions allow analytical resistance predictions of hot-rolled tube sections under fire.

Table 4: O.I.C. design coefficients for simple load cases.

Load case	λ_0	α_L	δ
N	0.40	$0.50 + 0.07 \cdot \gamma$	$0.65 - 0.10 \cdot \gamma \geq 0$
M_y	0.20	$0.08 + 0.06 \cdot \gamma$	$1.01 - 0.20 \cdot \gamma \geq 0$
M_z	0.40	$0.46 + 0.03 \cdot \gamma$	$0.007 + 0.110 \cdot \gamma$

Table 5: q_i factors for combined load cases.

q_1	q_2	q_3	q_4	q_5	q_6
0.98	3.04	2.8	2.2	2.3	1.95

4. Performance of O.I.C.-based proposals

4.1 Simple load cases

In this paragraph, resistance predictions for the proposed design approach are compared to the reference numerical results and to resistance estimates by well-known design codes: Eurocode 3 (EC3, (European Committee for Standardisation, 2020)), the American Specifications (A.I.S.C. (AISC, 2016)) and the Canadian Standards (C.S.A. (CSA, 2019)). Fig. 11a to 13b provide an overview of the results for simple load cases, i.e., compression N, major-axis M_y or minor-axis bending M_z. Figs. 11a, 12a and 13b plot the results in $\chi_L - \lambda_L$ axes, and resistance predictions obtained from F.E. simulations, from Eurocode 3, from the Canadian Standards C.S.A. and from the American Standards A.I.S.C. are presented. It is to be recalled that χ_L shall be seen as a direct indication of the resistance, since χ_L represents a "reduction factor" owing to buckling and imperfections on the plastic capacity, kept as a reference; therefore, vertical axes of these figures straightforwardly characterize resistance levels. Figs. 11b, 12b and 13b provide statistical information on the performance of each set of design recommendations $\chi_{L,\,Ref.}$ (where *Ref.* denotes

the design rules considered) relative to the F.E.-predicted resistance $\chi_{L\,F.E.}$. Accordingly, a value of $\chi_{L,\,Ref.}$ / $\chi_{L\,F.E.}$ lower than 1.0 indicates that the reference standard provides a safe resistance prediction, while a ratio larger than 1.0 exposes unsafety. These histograms allow to characterize both accuracy (highly accurate resistance predictions are characterized by $\chi_{L,\,Ref.}$ / $\chi_{L\,F.E.}$ ratios close to 1.0 – yet slightly lower to remain safe-sided) and consistency (distribution of predictions is steady and reliable, i.e., histogram is narrow).

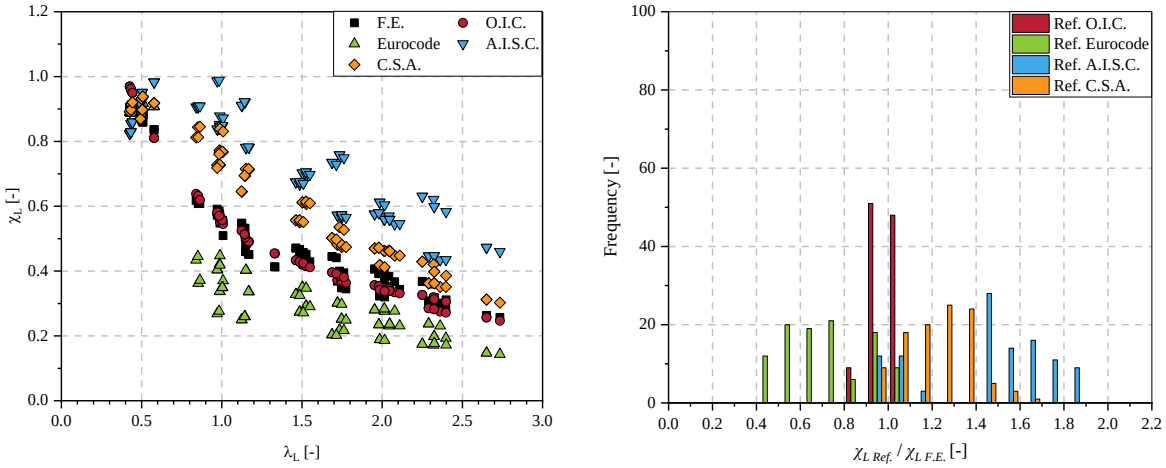

Figure 11: Results for sections under compression N – a) $\chi_L - \lambda_L$ O.I.C. plot – b) Frequency distribution.

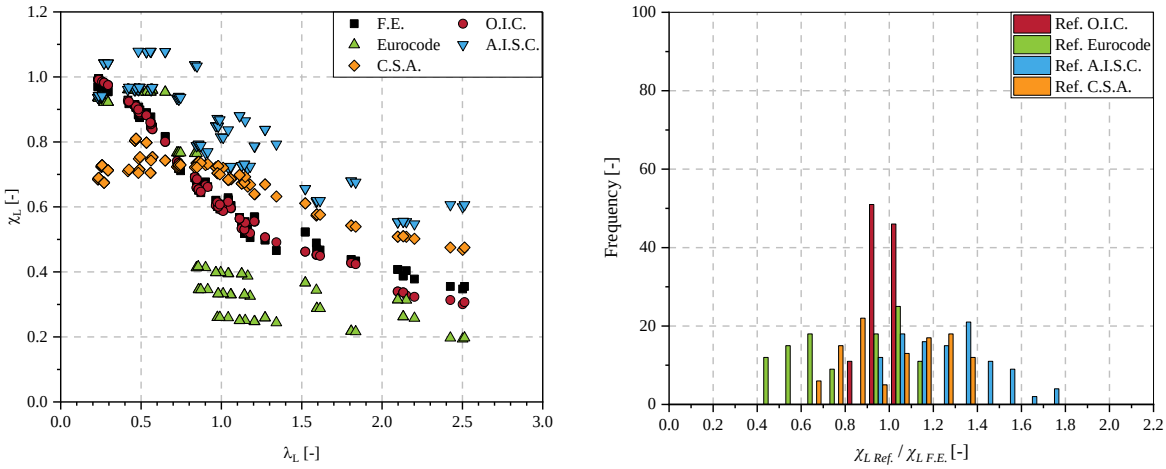

Figure 12: Results for sections under major-axis bending M_y – a) $\chi_L - \lambda_L$ O.I.C. plot – b) Frequency distribution.

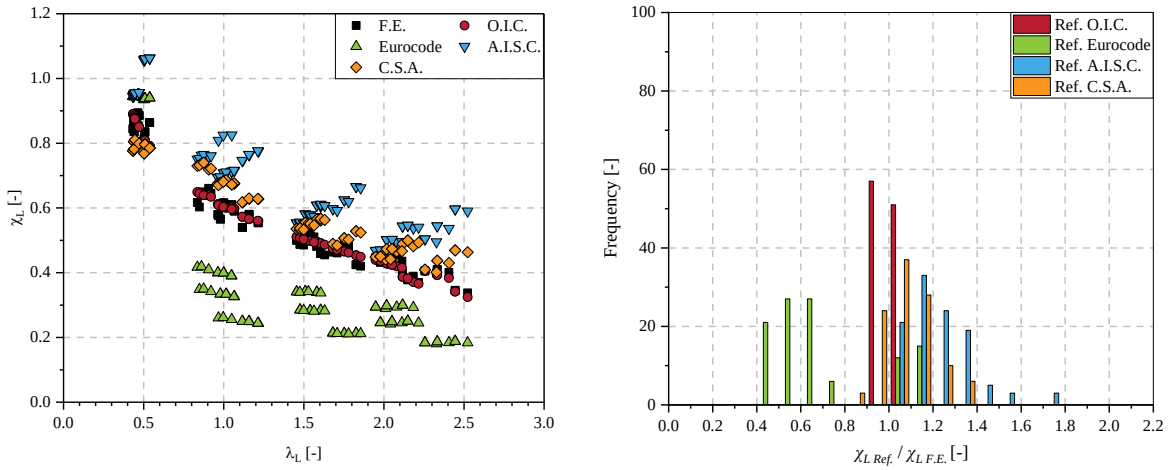

Figure 13: Results for sections under minor-axis bending M_z – a) $\chi_L - \lambda_L$ O.I.C. plot – b) Frequency distribution.

The following key observations can be made from these figures:

- The O.I.C. proposal provides very accurate, consistent and safe resistance estimates for each load case. In contrast, all other approaches lead to either significantly over-safe predictions (Eurocode 3) or unsafe predictions (C.S.A. and A.I.S.C.);
- Eurocode 3 is generally over-conservative, often providing capacities which could possibly be doubled (i.e., $\chi_{L,\,Ref.} / \chi_{L\,F.E.} \leq 0.5$), meaning that significant improvements can be foreseen. One of the reasons for the observed excessive safety stems from the fact that Eurocode 3 prescribes an extra reduction factor for member buckling as soon as the length gets higher than zero, even by a little amount, i.e., when only cross-section resistance prevails. Consequently, Eurocode 3 predictions unduly penalizes cross-sectional carrying capacities, causing the results to be more conservative than they should;
- A.I.S.C. design rules appear to be generally quite unsafe compared to F.E. results, in particular for compression. A plausible reason lies in the fact that A.I.S.C. uses different reduction factors for the mechanical properties at elevated temperatures than Eurocode 3 ones. As the F.E. results are based on the material properties under fire recommended by the Eurocode, this further questions the adequacy of both Eurocode and A.I.S.C. recommendations for steel properties at elevated temperatures. Also, A.I.S.C. relies on the 0.2% proof stress for slender sections, unlike for non-slender sections. Accordingly, the importance of local buckling might be underestimated and needs to be improved.

Table 6 provides another detailed view of the results and further confirms these observations: for compression cases, Eurocode 3 provides nearly 75% of its results with more than 10% safety. A.I.S.C. shows average values of the ratio $\chi_{L,\,A.I.S.C.} / \chi_{L\,F.E.}$ of 1.45, 1.26 and 1.23 for compression, major-axis bending and minor-axis bending cases, respectively, with a maximum ratio of 2.09 for compression, further emphasizing quite unsafe resistance estimates. Overall, despite its application simplicity, the O.I.C. provides a much higher performance than existing design approaches for simple load cases.

4.2 Combined load cases

This paragraph analyses results obtained for combined load cases, either compression + bending $N + M_y$ or $N + M_z$, biaxial bending $M_y + M_z$ or compression + biaxial bending $N + M_y + M_z$. As described in § 2.3, the relative bending-to-compression or major-to-minor axis ratios have been varied to span the entire set of possibilities, from compression-dominated to bending-dominant ones. Figs. 14a and 14b first summarize results for $N + M_y + M_z$ cases; further than evidencing a much larger scatter than for simple load cases, they reveal the same trends, i.e., Eurocode 3 is quite conservative, A.I.S.C. is mainly unsafe, C.S.A. is conservative for compact sections ($\lambda_L < 0.6$) yet unconservative for intermediate to large slenderness and the O.I.C.-based proposal provides excellent, accurate and consistent resistance predictions.

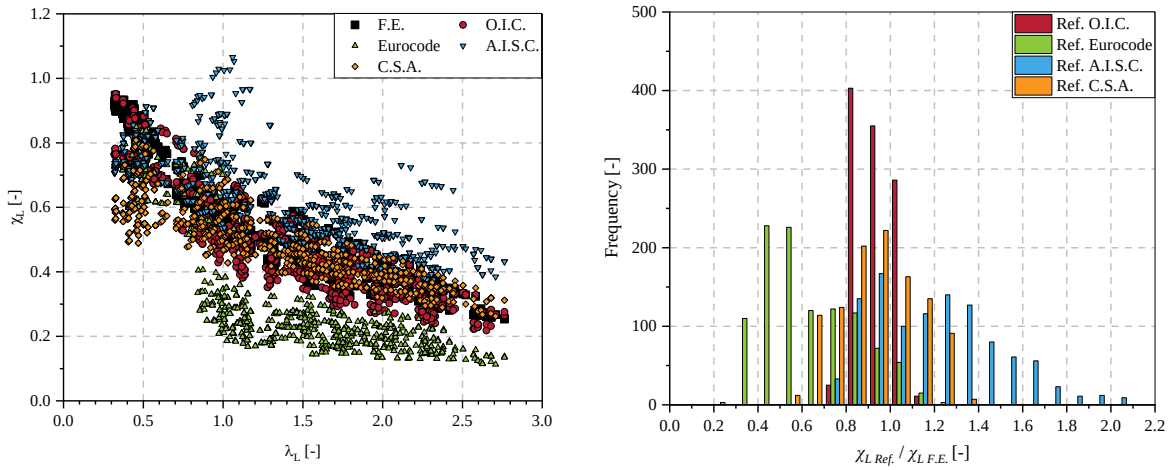

Figure 14: Results for sections under combined load cases $N + M_y + M_z$ – a) $\chi_L - \lambda_L$ O.I.C. plot – b) Frequency distribution.

Table 6 provides further insights on the results for combined load cases:

- The O.I.C. approach is overall very accurate: mean values of the $\chi_{L,\,O.I.C.} / \chi_{L\,F.E.}$ ratio vary from 0.91 to 1.00 for combined load cases, and this ratio for the whole set of 1 404 results considered is an excellent 0.95, meaning that the O.I.C.-based design equations lead to a 5% safety margin overall. This performance is nicely complemented by quite low Coefficients of Variation (C.o.V.) values, around 8% in average, further indicating a high level of consistency, i.e., the ability to provide resistance estimates quite close to the reference F.E. ones. Too, over more than 1 400 results, the worst unsafe prediction amounts 12% while the worst over-conservative one is 22%. Fig. 16b offers a visual confirmation of these observations, where for all considered load cases (both simple and combined), the ability of this approach to provide precise and reliable resistance estimates ($\chi_{L,\,O.I.C.} \approx \chi_{L\,F.E.}$) is obvious. Given the number, variety and complexity of the cases considered here, the performance of the proposed approach is evidenced to be excellent;
- A.I.S.C. resistance predictions are confirmed to be quite over-optimistic, in the same order of magnitude reported for simple load cases (≈ 25% unsafety in average, at the exception of the $M_y + M_z$ biaxial bending case, which further indicates that compression-dominated cases may constitute the biggest challenge: recall the mean $\chi_{L,\,A.I.S.C.} / \chi_{L\,F.E.}$ ratio of 1.45 for simple compression). The worst unsafe ratio is as high as 2.09, meaning that A.I.S.C. overestimates the true capacity by more than a factor 2 in this case. Combined, these results

reveal that typical safety factors providing a 10% safety margin ($\phi = 0.90$ in A.I.S.C. standards or $\gamma_{M0} = 1.10$ in Eurocode terminology) will show far insufficient to ensure safe design resistances. In addition, C.o.V.s are generally quite high, with a 22.8% average. Fig. 15a further illustrates (i) generally unsafe resistance predictions and (ii) quite scattered results;

- C.S.A. results (see also Fig. 15b) are seen mostly unsafe for compression N or M_z cases (mean values of 1.22 and 1.08 and Max. ratios of 1.63 and 1.36, respectively) yet over-conservative for $M_y + M_z$ or $N + M_y + M_z$ cases (means values of 0.79 and 0.89, respectively) – a more detailed look at the results indicates that slender sections under M_y are associated to over-safe predictions, as Fig. 12a also showed;
- Eurocode 3, for all 1 404 cases, is quite overconservative with an average of 0.66. Whatever the load case considered, either simple or combined, EC3 averages of the $\chi_{L,\,EC3}$ / $\chi_{L\,F.E.}$ ratio are very low. Too, C.o.V.s are always the highest among all design rules, indicating a rather poor performance in terms of consistency;
- Some of the last columns in Table 6 are meant at characterizing overconservativeness: column "< 0.90 [%]" indicates the percentage of results that are safer than 10%, while column "< 0.75 [%]" relates to very conservative results (proportion of results offering more than 25% safety, i.e., ratio $\chi_{L,\,Ref.}$ / $\chi_{L\,F.E.} < 0.75$). For example, the O.I.C. proposal provides some 31.9% results out of 1 404 which are more than 10% safe, yet 0% of the $\chi_{L,\,O.I.C.}$ / $\chi_{L\,F.E.}$ ratio lower than 0.75, which means that this proposal can be safe but not exaggeratedly safe. In contrast, Eurocode 3 offers about 82% of its predictions safer than 10%, and 67% of them offer more than 25% over-conservativeness. C.S.A. resistance predictions are seen not to be overly conservative, while A.I.S.C. has very little resistance estimate on the safe side (only 12% lower than 0.90 and none below 0.75);
- Oppositely, the last 3 columns in Table 6 are relative to unsafe resistance predictions: column "> 1.03 [%]" identifies slightly unsafe predictions – which may be not considered as problematic –, column "> 1.10 [%]" reports on unsafe results who cannot be compensated by usual safety factors (see next section) and column "> 1.25 [%]" points out severely unsafe resistance estimates (more than 25% resistance over-prediction). In this respect, A.I.S.C. rules are seen to be quite problematic, since large proportions of the results are seen beyond a ratio of 1.25: 44% in average, and as high as 74% for simple compression cases. The performance of Eurocode 3 with respect to unsafe predictions is generally good (a small amount of predictions exceed ratios of 10% unsafety – only 3.2% overall), whereas the Canadian Standards C.S.A. are not: some 40% or all results exceed 10% unsafety. A detailed analysis of the results indicate that compression-dominated cases may be the source of the unconservativeness and that the interaction format for $N + M_y + M_z$ cases seems inappropriate, since the ratios $\chi_{L,\,C.S.A.}$ / $\chi_{L\,F.E.}$ drop considerably whereas it does not for other cases. In contrast, the O.I.C. proposal offers excellent resistance predictions, with only 0.8% of the total results beyond 10% unsafety, i.e., a usual safety factor $\gamma_{M0} = 1.10$ shall get almost all results back to safe predictions. More details on reliability aspects are provided in Section 4.3.

Figs. 15a to 16b offer a visual assessment of all results for all load cases. They plot $\chi_{L,\,Ref.}$ / $\chi_{L\,F.E.}$ ratios on the vertical axes and are sorted as a function of the load combination. They further illustrate that (i) A.I.S.C. is generally unsafe and inconsistent, whatever the load case considered (Fig. 15a), that (ii) C.S.A. (Fig. 15b) offers a little more consistent resistance predictions yet both over-conservative and unsafe, that (iii) Eurocode 3 leads to safe-sided and scattered predictions (Fig. 16a) and that (iv) the O.I.C. approach (Fig. 16b) offers significantly better resistance estimates, both in terms of accuracy and consistency, and has virtually no outliers, whatever the load case considered.

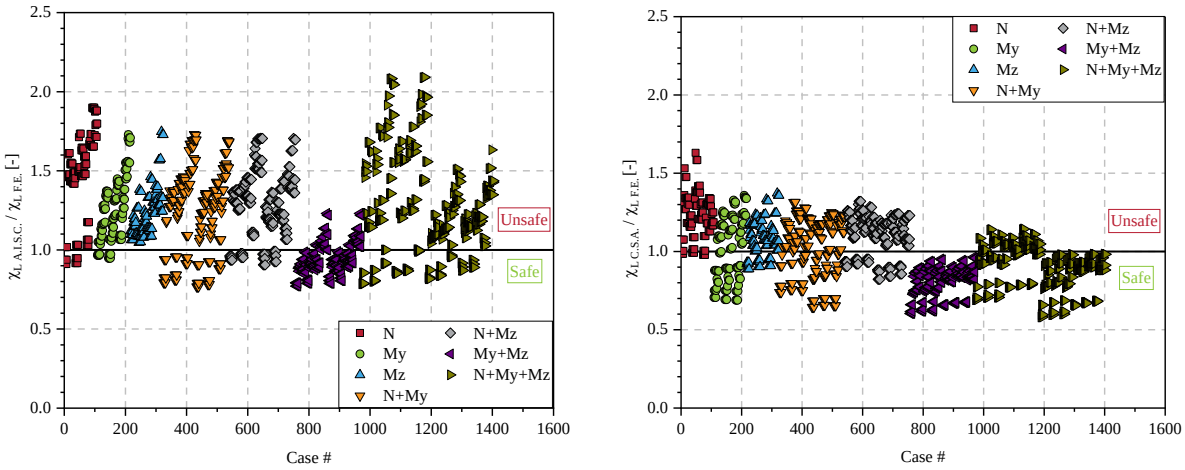

Figure 15: Performance of design proposals for all load cases – a) A.I.S.C. – b) C.S.A.

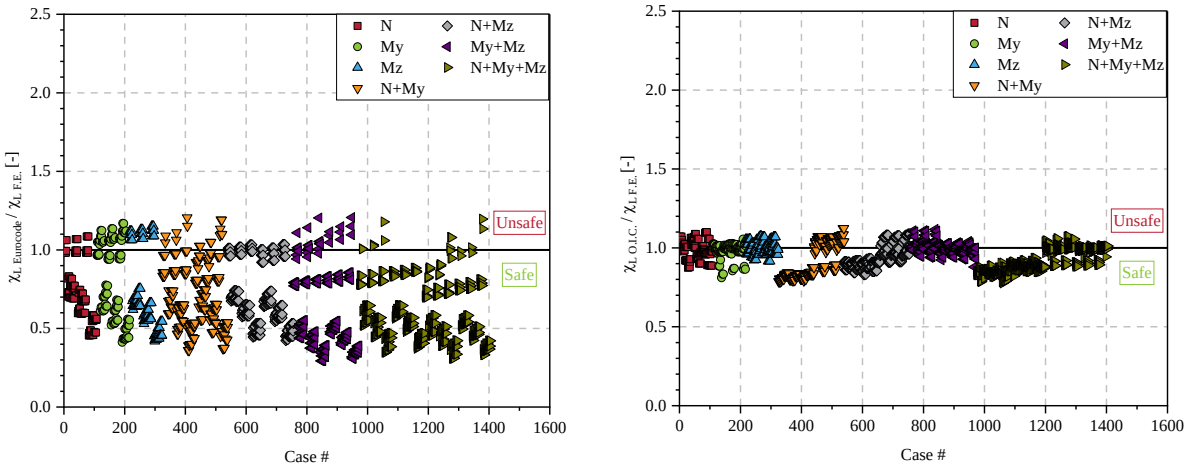

Figure 16: Performance of design proposals for all load cases – a) Eurocode 3 – b) O.I.C. proposal.

Table 6: detailed results of comparison F.E. results vs other design proposals.

Load cases	Number of cases	Proposals	Mean	C.o.V.	Max.	Min.	< 0.90 [%]	< 0.75 [%]	> 1.03 [%]	> 1.10 [%]	> 1.25 [%]
All load cases	1 404	O.I.C.	0.95	8.3%	1.12	0.78	31.9%	0.0%	13.2%	0.8%	0.0%
		EC3	0.66	33.1%	1.21	0.29	81.9%	67.0%	8.3%	3.2%	0.0%
		C.S.A.	0.98	19.5%	1.63	0.58	35.8%	12.1%	40.9%	28.9%	6.3%
		A.I.S.C.	1.23	22.8%	2.09	0.77	12.1%	0.0%	72.3%	63.3%	43.9%
Compression N	108	O.I.C.	0.99	6.0%	1.10	0.87	8.3%	0.0%	24.1%	0.0%	0.0%
		EC3	0.74	25.5%	1.09	0.45	74.3%	60.0%	8.6%	0.0%	0.0%
		C.S.A.	1.22	12.3%	1.63	0.98	0.0%	0.0%	82.9%	74.3%	40.0%
		A.I.S.C.	1.45	20.3%	1.90	0.91	0.0%	0.0%	82.9%	77.1%	74.3%
Major-axis bending M_y	108	O.I.C.	0.98	4.8%	1.06	0.81	10.2%	0.0%	0.9%	0.0%	0.0%
		EC3	0.81	30.1%	1.17	0.41	50.0%	47.2%	33.3%	10.2%	0.0%
		C.S.A.	1.02	20.5%	1.36	0.69	39.8%	11.1%	52.8%	43.5%	12.0%
		A.I.S.C.	1.26	15.9%	1.73	0.95	0.0%	0.0%	88.9%	72.2%	50.9%
Minor-axis bending M_z	108	O.I.C.	1.00	4.2%	1.07	0.92	0.0%	0.0%	22.2%	0.0%	0.0%
		EC3	0.71	34.8%	1.15	0.42	75.0%	72.2%	25.0%	13.9%	0.0%
		C.S.A.	1.08	11.0%	1.37	0.89	2.8%	0.0%	66.7%	40.7%	5.6%
		A.I.S.C.	1.23	12.1%	1.75	1.05	0.0%	0.0%	100.0%	80.6%	38.9%
$N + M_y$	216	O.I.C.	0.91	12.1%	1.12	0.79	62.5%	0.0%	27.8%	0.9%	0.0%
		EC3	0.70	29.0%	1.21	0.36	80.6%	62.1%	6.8%	3.4%	0.0%
		C.S.A.	1.03	18.1%	1.32	0.64	26.7%	10.2%	57.3%	46.6%	4.4%
		A.I.S.C.	1.26	21.2%	1.73	0.77	13.1%	0.0%	76.7%	72.3%	59.7%
$N + M_z$	216	O.I.C.	0.93	6.8%	1.09	0.83	30.6%	0.0%	11.6%	0.0%	0.0%
		EC3	0.69	27.8%	1.03	0.42	75.0%	75.0%	2.8%	0.0%	0.0%
		C.S.A.	1.10	11.6%	1.32	0.82	9.7%	0.0%	75.0%	56.9%	7.9%
		A.I.S.C.	1.28	16.2%	1.71	0.91	0.0%	0.0%	83.3%	79.2%	59.7%
$M_y + M_z$	216	O.I.C.	1.00	3.9%	1.12	0.88	0.5%	0.0%	16.2%	4.2%	0.0%
		EC3	0.61	40.7%	1.21	0.29	86.1%	61.1%	7.4%	3.7%	0.0%
		C.S.A.	0.79	12.1%	0.96	0.60	88.4%	29.6%	0.0%	0.0%	0.0%
		A.I.S.C.	0.94	10.7%	1.23	0.77	36.1%	0.0%	19.9%	6.0%	0.0%
$N + M_y + M_z$	432	O.I.C.	0.92	7.6%	1.07	0.78	52.3%	0.0%	3.2%	0.0%	0.0%
		EC3	0.60	30.9%	1.20	0.31	95.4%	73.6%	1.6%	0.7%	0.0%
		C.S.A.	0.89	15.4%	1.14	0.58	42.8%	16.7%	16.9%	3.2%	0.0%
		A.I.S.C.	1.27	24.7%	2.09	0.79	14.6%	0.0%	77.1%	69.9%	42.6%

4.3 Reliability analyses

Since every design approach shall be paired with a safety factor (either denoted as γ_{M0} for sections in Eurocode context or ϕ in the A.I.S.C. framework – $\gamma_{M0} \approx 1 / \phi$), reliability analyses towards the determination of such safety factors have been undertaken for all considered proposals. In this respect, the guidelines of Annex D of EN 1990 ((EN 1990, 2002)) have been considered – they are known to consider a little tighter safety levels than A.I.S.C. Typically, for cross-section resistance, an expected value for γ_{M0} is such that $\gamma_{M0} < 1.10$, indicating that a 10% extra safety is necessary to account for uncertainties related to material properties, section dimensions, and design model inaccuracies. In this study, a simplified approach (Taras, 2016) was used to determine γ_{M0} values. The key statistical parameters are detailed in Table 7, in which $K_{d,n}$ is the design fractile factor, b is the least squares estimator of the regression slope, V_d is the C.o.V. of the error's terms and V_r is the combined C.o.V. involving various uncertainties, calculated using Eqs. (4) and (5), where the C.o.V. of material strength V_{mat} was taken from Annex E of EN 1993-1-1 (PrEN 1993, 2018) and the C.o.V. of geometric properties V_{geom} was set equal to 0.03, as recommended in (Byfield, 1997).

$$V_r^{\,2} = V_\delta^{\,2} + V_{rt}^{\,2} \tag{4}$$

$$V_{rt}^{\,2} = V_{mat}^{\,2} + V_{geom}^{\,2} \tag{5}$$

The results are shown in the last column of Table 7: as can be observed, all design approaches but the O.I.C. fail to report γ_{M0} values lower than 1.10; rather high values of 1.75, 1.64 and 2.30 are reported for EC3, C.S.A. and A.I.S.C., respectively, whereas $\gamma_{M0\ O.I.C.} = 1.07$. This demonstrates the improved reliability and consistency of the O.I.C., establishing it as an appropriate design approach.

In an attempt to reach more satisfactory γ_{M0} values, so-called "tail approximations" (Taras, 2016) were performed to analyze how γ_{M0} varies with the number of data points considered in the tail. Fig. 17a illustrates the tail approximation technique on the particular case of Eurocode 3, where only 112 data points out of 1 404 were kept in the tail; in this figure, r_e represents the resistance obtained from F.E. simulations and r_t refers to EC3 estimates. The vertical axis, which standardizes the data by converting cumulative probabilities into corresponding standard deviation values, facilitates a normalized comparison of the distribution. The straight regression lines represent ideal cases where resistance function results perfectly follow a log-normal distribution, meaning all data points would align along it. Fig. 17b presents an overall plot of how γ_{M0} evolves with the number of data kept in the tail approximation, for the O.I.C. design approach and for the other design methods, using the same parameters (V_r, V_{mat}, V_{geom}) previously defined. The minimum safety factors obtained are reported in Table 8. As can be observed, all tail approximations lead to more satisfactory, γ_{M0} values. Nevertheless, although EC3 tailed safety factor comes close to 1.10 (1.11), all design codes γ_{M0} still fail to meet the expected requirements, in large amounts (in particular A.I.S.C. with a best (minimum) $\gamma_{M0\ A.I.S.C.\ tailed} = 1.89$). Conversely, the O.I.C. improves to $\gamma_{M0} = 1.01$ if 749 results are kept in the tail, further evidencing its robustness and reliability.

Table 7: Statistical results of $\chi_{L,Ref.}$ / $\chi_{L,\,F.E.}$ ratio for different proposals (all results considered).

Proposals	$K_{d,n}$	b	V_δ	V_r	γ_{M0}
O.I.C.	3.097	1.053	0.083	0.098	1.07
EC3	3.097	1.385	0.338	0.342	1.75
C.S.A.	3.097	0.977	0.203	0.209	1.64
A.I.S.C.	3.097	0.752	0.229	0.235	2.30

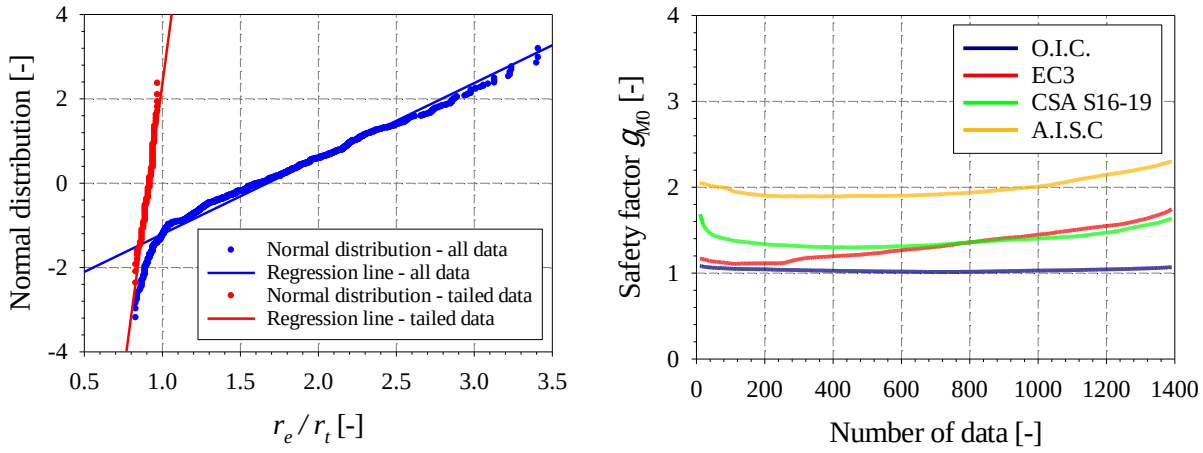

Figure 17: a) Example of tail approximation for EC3 with 112 data points – b) Evolution of safety factors with number of data kept in tail approximations.

Table 8: Minimum safety factor γ_{M0} according to best tail approximation for different proposals.

Proposals	n_{tail}	γ_{M0}
O.I.C.	749	1.01
EC3	112	1.11
C.S.A.	451	1.30
A.I.S.C.	360	1.89

5. Conclusions

This paper detailed an original approach to the cross-section resistance of hot-rolled rectangular and square hollow shapes at high temperatures. In a 1st step, advanced non-linear shell F.E. models were developed then validated against 17 carefully-conducted and fully documented tests. As the numerical models showed an excellent ability to reproduce physical testing (peak loads, stiffness, post-buckling behaviour and failure modes), they have been used extensively to collect more than 1 400 numerical results varying cross-section dimensions, temperature and load cases. They served as a reference to assess the merits of an original, O.I.C.-based design proposal. The latter consists in an extension of the well-known resistance-stability interaction used for member buckling to local, cross-section buckling. Systematic comparison with the F.E. results and resistance estimates from major design standards were then described, and the O.I.C. approach was evidenced to offer a quite superior performance than all other codes in terms of accuracy, consistency and safety, despite being simpler in application. The main reasons lie in (i) a strong, mechanically-based background, (ii) the possibility to rely on numerical tools for the determination of key coefficients (R_{pl} and $R_{cr,L}$) and (iii) adequate, refined definitions of local buckling curves $\chi_L = f°(\lambda_L)$. Eventually, investigations towards characterizing the safety levels of all the design rules considered allowed to conclude that all design recommendations but the O.I.C. proposal fail to satisfy the usual 10% safety level expected for cross-section resistance.

References

Abaqus G. (2011). Abaqus 6.11. Providence, RI, USA: Dassault Systemes Simulia Corporation.

Afshan S, Gardner L. (2013). The continuous strength method for structural stainless steel design. Thin-Walled Struct;68:42–9.

AISC. ANSI/AISC 360–16 – specification for structural steel buildings (2016). Chicago, Ill: American Institute of Steel Construction.

Aleseyedan, M. (2023), "O.I.C.-Based Design of Steel H.S.S. at High Temperatures," MSc Thesis, Civil and Water Engineering Department, Laval University.

W. E. Ayrton and J. Perry. (1886). "On struts", The Engineer, vol. 62.

Boissonnade N, Nseir J, Saloumi E. (2013). The Overall Interaction Concept: an Alternative Approach to the Stability and Resistance of Steel Sections and Members. Proceedings. 2013 SSRC Annual Stability Conference, Saint Louis, USA.

Boissonnade N, Nseir J, Hayeck M, Saloumi E. (2014). Predicting steel member carrying capacity by means of the Overall Interaction Concept. Proceedings. 7th European Conference on Steel Structures, Eurosteel 2014, Naples, Italy.

Boissonnade N. (2015). Application of the Overall Interaction Concept to the Design of Steel Sections and Members. Proceedings. 9th European Solid Mechanics Conference ESMC-2015, Madrid, Spain.

Boissonnade N, Hayeck M, Saloumi E, Nseir J. (2017). An overall interaction concept for an alternative approach to steel members design. J Constr Steel Res;135:199–212.

Byfield, M. P. and Nethercot, D. A. (1997). "Material and geometric properties of structural steel for use in design". Structural Engineer, Vol. 75, No. 21.

CSA Group: Standard Council of Canada. (2019)., "CSA S16:19: Design of steel structures," Toronto, Canada, p. 306.

Chen J, Young B. (2008). Design of high strength steel columns at elevated temperatures. J Constr Steel Res;64(6):689–703.

Couto C, Vila Real P, Lopes N, Zhao B. (2014). Effective width method to account for the local buckling of steel thin plates at elevated temperatures. Thin-Walled Struct;84:134–49.

C. Couto, P. Vila Real, N. Lopes, and B. Zhao (2015). 'Resistance of steel cross-sections with local buckling at elevated temperatures', Journal of Constructional Steel Research, vol. 109, pp. 101–114, doi: 10.1016/j.jcsr.2015.03.005.

C. Couto, P. Vila Real, N. Lopes, and B. Zhao. (2016). 'Numerical investigation of the lateral–torsional buckling of beams with slender cross sections for the case of fire', Engineering Structures, vol. 106, pp. 410–421, doi: 10.1016/j.engstruct.2015.10.045.

C. Couto, T. Coderre, P. Vila Real, and N. Boissonnade. (2021). 'Cross-section capacity of RHS and SHS at elevated temperatures: Comparison of design methodologies', Structures, vol. 34, pp. 198–214, doi: 10.1016/j.istruc.2021.07.072.

EN 1990 (2002). Basis of Structural Design. Brussels: European Committee for Standardization.

PrEN 1993-1-1. (2018). Eurocode 3 - Design of Steel Structures - Part 1-1: General Rules and Rules for Buildings, European Committee for Standardization (CEN).

CEN. EN 1993-1-2 (2005). Eurocode 3: Design of steel structures - Part 1-2: General rules - Structural fire design.

European Committee for Standardisation (CEN). (2020). PrEN 1993-1-2: Eurocode 3 - Design of steel structures - part 1–2: General rules-structural fire design.

Fang H, Chan T-M. (2018). Axial compressive strength of welded S460 steel columns at elevated temperatures. Thin-Walled Struct;129:213–24.

Fang, H., Chan, T.M. (2019). Resistance of axially loaded hot-finished S460 and S690 steel square hollow stub columns at elevated temperatures. Structures, 17:66–73.

Franssen J-M, Vila Real P. (2015). Fire Design of Steel Structures. ECCS Press, and Ernst & Sohn a Wiley Company.

Gagné A-S, Gérard L, Boissonnade N. (2020). Design of stainless steel cross-sections for simple load cases with the O.I.C. Journal of Constructional Steel Research. 168. http://dx.doi.org/https://doi.org/10.1016/j.jcsr.2020.105936.

Gérard L, Li L, Kettler M, Boissonnade N. (2021). Steel I-sections resistance under compression or bending by the Overall Interaction Concept. Journal of Constructional Steel Research. 182. http://dx.doi.org/https://doi.org/10.1016/j.jcsr.2021.106644.

M. Hayeck (2016). "Development of a new design method for steel hollow section members resistance", PhD thesis, University Of Applied Sciences Of Western Switzerland - Fribourg, University of Liège, Saint-Joseph University Beirut.

Hayeck M, Saloumi E, Nseir J, Boissonnade N. (2017). Stability and Resistance of Hollow Section Steel Beam-Columns. Proceedings. 2017 SSRC Annual Stability Conference, San Antonio, USA.

Hayeck M, Nseir J, Saloumi E, Boissonnade N. (2018). Experimental characterization of steel tubular beam-columns resistance by means of the Overall Interaction Concept. Thin-walled Structures. 128:92-107. http://dx.doi.org/10.1016/j.tws.2017.05.019.

Knobloch M, Fontana M. (2006). Strain-based approach to local buckling of steel sections subjected to fire. J Constr Steel Res;62(1–2):44–67.

M. Knobloch (2007). 'Local Buckling Behaviour of Steel Sections Subjected to Fire', Fire Science and Technology, vol. 26, no. 2, pp. 61–66, doi:10.3210/fst.26.61.

M. Knobloch, J. Pauli, D. Somaini, and M. Fontana (2013). 'Stress–strain response and cross-sectional capacity of steel sections in fire', Proceedings of the Institution of Civil Engineers - Structures and Buildings, vol. 166, no. 8, pp. 444–455, doi: 10.1680/stbu.12.00061.

M. Knobloch (2014). 'Stability of steel structures in fire: State-of-the-art, recent studies in Switzerland and future trends', Stahlbau, vol. 83, no. 4, pp. 257–264, doi: 10.1002/stab.201410147.

V. Kodur, M. Dwaikat, and R. Fike (2010). 'High-Temperature Properties of Steel for Fire Resistance Modeling of Structures', J. Mater. Civ. Eng., vol. 22, no. 5, pp. 423–434, doi: 10.1061/(ASCE)MT.1943-5533.0000041.

Kucukler M. (2021). Local stability of normal and high strength steel plates at elevated temperatures. Eng Struct;243:112528.

Li , L; Boissonnade, N. (2022a). Design of mono-symmetric I-sections under combined load cases by the Overall Interaction Concept. Thin-Walled Structures. http://dx.doi.org/https://doi.org/10.1016/j.tws.2022.110280.

Li, L; Fafard, F; Boissonnade, N. (2022b). Local and global instabilities of rolled T-sections under axial compression. Thin-Walled Structures. 178: 109517. http://dx.doi.org/https://doi.org/10.1016/j.tws.2022.109517.

Li, L; Gérard, L; Kettler, M; Boissonnade, N. (2022c). The Overall Interaction Concept for the design of hot-rolled and welded I-sections under combined loading. Thin-Walled Structures. 172: 108623. http://dx.doi.org/https://doi.org/10.1016/j.tws.2021.108623.

Li, L; Gérard, L; Langlois, S; Boissonnade, N. (2022d). O.I.C.-based design of mono-symmetric I-sections under simple load cases. Thin-Walled Structures. 174: 109134. http://dx.doi.org/https://doi.org/10.1016/j.tws.2022.109134.

Li, L; Boissonnade, N. (2022e). Local/global coupled instabilities of slender I-sections under compression. Thin-Walled Structures. 172: 108842. http://dx.doi.org/https://doi.org/10.1016/j.tws.2021.108842.

Li, L; Paquet, J; Couto, C; Vila Real, P; Boissonnade, N. (2023a). Fire local stability of steel I-sections under simple load cases. Engineering Structures. 283: 115874. http://dx.doi.org/https://doi.org/10.1016/j.engstruct.2023.115874.

Li, L; Dahboul, S; Verma, P; Dey, P; Fafard, M; Boissonnade, N. (2023b). O.I.C.-Based Design of Aluminum Circular Hollow Sections under Compression or Pure Bending. Engineering Proceedings. 43(31). http://dx.doi.org/https://doi.org/10.3390/engproc2023043031.

Li, L; Coderre, T; Boissonnade, N. (2023c). O.I.C.-based design of extruded and welded aluminum I-sections. Structures.

Li, L; Paquet, J; Couto, C; Vila Real, P; Boissonnade, N. (2023d). Fire local stability of steel I-sections under simple load cases. Engineering Structures. 283: 115874. http://dx.doi.org/https://doi.org/10.1016/j.engstruct.2023.115874.

Li, L; Paquet, J; Couto, C; Vila Real, P; Boissonnade, N. (2023e). Improved fire design of steel I-sections under combined compression and bending. Structures. 53: 346-360. http://dx.doi.org/https://doi.org/10.1016/j.istruc.2023.04.021.

K. T. Ng and L. Gardner (2007). 'Buckling of stainless steel columns and beams in fire', Engineering Structures, vol. 29, no. 5, pp. 717–730, doi: 10.1016/j.engstruct.2006.06.014.

R. Maquoi and J. Rondal. (1978). "Mise en équation des nouvelles courbes européennes de flambement", Construction Métallique, no. 1, pp. 17-29.

Nseir J, Saloumi E, Hayeck M, Taras A, Boissonnade N. (2014). An alternative approach for the prediction of hollow structural shapes cross-sectional resistance: the Overall Interaction Concept. Proceedings. 2014 SSRC Annual Stability Conference, Toronto, Canada.

J. Nseir (2015a). "Development of a new design method for the cross-section capacity of steel hollow sections", PhD thesis, University Of Applied Sciences Of Western Switzerland - Fribourg, University of Liège, Saint-Joseph University Beirut.

Nseir J, Saloumi E, Hayeck M, Boissonnade N. (2015b). A new design method for hollow steel sections: the Overall Interaction Concept. Proceedings. 15th International Symposium on Tubular Structures, ISTS15, Rio de Janeiro, Brasil.

Nseir J, Hayeck M, Saloumi E, Boissonnade N. (2015c). Practical design of hollow structural shapes by means of the Overall Interaction Concept. Proceedings. 2015 SSRC Annual Stability Conference, Nashville, USA.

Nseir J, Hayeck M, Saloumi E, Boissonnade N. (2016). Influence of imperfections on the local buckling response of hollow structural shapes. Proceedings. 2016 SSRC Annual Stability Conference, Orlando, USA.

J. Pauli, D. Somaini, M. Knobloch, and M. Fontana (2012), 'Experiments on steel columns under fire conditions', p. 124 S., doi: 10.3929/ETHZ-A-007600651.

Pauli J. (2013). The behaviour of steel columns in fire: material – cross-sectional capacity-column buckling. PhD thesis, Swiss Federal Institute of Technology Zurich.

S. E. Quiel and M. E. M. Garlock (2010). 'Calculating the buckling strength of steel plates exposed to fire', Thin-Walled Structures, vol. 48, no. 9, pp. 684–695, doi: 10.1016/j.tws.2010.04.001.

Renaud C, Zhao B. (2006). Investigation of the simple calculation method in EN 1993-1-2 for buckling of hot rolled class 4 steel members exposed to fire. In: Proceedings of the fourth international workshop "Structures in Fire". p. 199–211.

D. Somaini (2012). 'Biegeknicken und Lokalles Beulen von Stahlstützen im Brandfall'. PhD Thesis, ETH Zürich.

Taras, A., Dehan, V., da Silva, L. S., Marques, L., and Tankova, T. (2016) "SAFEBRICTILE: Standardization of Safety Assessment Procedures across Brittle to Ductile Failure Modes".

Theofanous M, Propsert T, Knobloch M, Gardner L. (2016). The continuous strength method for steel cross-section design at elevated temperatures. Thin-Walled Struct;98:94–102.

P. M. M. Vila Real, R. Cazeli, L. Simões da Silva, A. Santiago, and P. Piloto. (2004). 'The effect of residual stresses in the lateral-torsional buckling of steel I-beams at elevated temperature', Journal of Constructional Steel Research, vol. 60, no. 3–5, pp. 783–793, doi: 10.1016/S0143-974X(03)00143-3.

Von Karman T., Sechler E.E., Donnell L.H. (1932). The strength of thin plates in compression. Trans Am Soc Mech Eng;54:53.

Winter G. (1947). Strength of thin steel compression flanges. Trans Am Soc Mech Eng;112:527.

K.-C. Yang and R. Hsu. (2009) ‘Structural behavior of centrally loaded steel columns at elevated temperature’, Journal of Constructional Steel Research, vol. 65, no. 10–11, pp. 2062–2068, doi: 10.1016/j.jcsr.2009.06.007.

X. Yun, N. Saari, and L. Gardner (2020). ‘Behaviour and design of eccentrically loaded hot-rolled steel SHS and RHS stub columns at elevated temperatures’, Thin-Walled Structures, vol. 149, p. 106646, doi: 10.1016/j.tws.2020.106646.